Physics Letters B 808 (2020) 135626

Contents lists available at ScienceDirect

Physics Letters B

www.elsevier.com/locate/physletb

Zeptosecond contact times for element Z=120 synthesis

H.M. Albers [a,*], J. Khuyagbaatar [a,b], D.J. Hinde [c], I.P. Carter [c], K.J. Cook [c,1], M. Dasgupta [c], Ch.E. Düllmann [a,b,d], K. Eberhardt [b,d], D.Y. Jeung [c], S. Kalkal [c,2], B. Kindler [a], N.R. Lobanov [c], B. Lommel [a], C. Mokry [b,d], E. Prasad [c,3], D.C. Rafferty [c], J. Runke [a], K. Sekizawa [e,f], C. Sengupta [c], C. Simenel [c,g], E.C. Simpson [c], J.F. Smith [c,4], P. Thörle-Pospiech [b,d], N. Trautmann [d], K. Vo-Phuoc [c], J. Walshe [c], E. Williams [c], A. Yakushev [a]

[a] GSI Helmholtzzentrum für Schwerionenforschung, 64291, Darmstadt, Germany
[b] Helmholtz Institute Mainz, 55099, Mainz, Germany
[c] Department of Nuclear Physics, Research School of Physics, Australian National University, Canberra, ACT 2601, Australia
[d] Johannes Gutenberg-Universität Mainz, 55099, Mainz, Germany
[e] Center for Transdisciplinary Research, Institute for Research Promotion, Niigata University, Niigata 950-2181, Japan
[f] Division of Nuclear Physics, Center for Computational Sciences, University of Tsukuba, Ibaraki 305-8577, Japan
[g] Department of Theoretical Physics, Research School of Physics, Australian National University, Canberra, ACT 2601, Australia

ARTICLE INFO

Article history:
Received 29 May 2020
Received in revised form 13 July 2020
Accepted 13 July 2020
Available online 17 July 2020
Editor: B. Blank

Keywords:
Superheavy-element formation
Z=120
Quasifission

ABSTRACT

The synthesis of new superheavy elements beyond oganesson (Z=118) requires fusion reactions with projectile nuclei with proton numbers larger than that of ^{48}Ca (Z=20), which has been successfully employed for the synthesis of elements with Z=112-118. In such reactions, fusion is drastically hindered by fast non-equilibrated dynamical processes. Attempts to produce nuclei with Z=120 using the ^{64}Ni+^{238}U, ^{58}Fe+^{244}Pu, ^{54}Cr+^{248}Cm, and ^{50}Ti+^{249}Cf reactions have been made, which all result in larger Coulomb forces than for ^{48}Ca-induced reactions, but no discovery has been confirmed to date. In this work, mass and angle distributions of fission fragments from these reactions have been measured with large angular coverage to aid in selection of the most promising projectile-target combination that would favor fusion. The results yield information on reaction contact times, with the longest exhibited by ^{50}Ti+^{249}Cf.

1. Introduction

The search for new elements represents one of the main focus points of physics research. To date, all of the elements with atomic number Z≤118 have been discovered, accessing the locality of the so-called island of stability - a region of superheavy nuclei (SHN) with enhanced stability due to shell closures, predicted more than half a century ago [1,2]. Expectations of the locations of these shell closures vary, with early calculations predicting 'new' magic shells to appear at Z=114 and N=184 [3]. Most modern calculations predict closed proton shells at Z=114, 120, 124 or 126 and a neutron shell closure at N=172 and/or 184 (e.g., [4–8]). No clear indications of such a shell closure at Z=114 have yet been observed, giving a strong motivation to push to ever-heavier elements.

New beam and target combinations must be explored to reach beyond Z=118 as doubly-magic ^{48}Ca projectile ions, successfully used in fusion-evaporation reactions for the production of elements with Z=112-118 [9–24], cannot presently be used due to insufficient amounts of target material with Z>98 [25]. Campaigns totaling about one year of accelerator beamtime searching for the element with Z=120 have been carried out using the ^{64}Ni+^{238}U [26], ^{58}Fe+^{244}Pu [27], ^{54}Cr+^{248}Cm [28,29] and ^{50}Ti+^{249}Cf [30,31] fusion-evaporation reactions. Despite this, element Z=120 remains undiscovered, suggesting that production cross sections are lower than those for ^{48}Ca-induced reactions. However, the important question of how much lower the production cross sections are remains unanswered, which is a critical issue for the planning of successful future SHN experiments.

* Corresponding author.
E-mail address: h.albers@gsi.de (H.M. Albers).

[1] Present address: Facility for Rare Isotope Beams, Michigan State University, East Lansing, Michigan 48824, USA.

[2] Present address: School of Physics and Material Sciences, Thapar University, Patiala-147004, India.

[3] Present address: Department of Physics, School of Mathematical and Physical Sciences, Central University of Kerala, Kasaragod-671314, India.

[4] Present address: Advanced Technology Institute, University of Surrey, Guildford, Surrey, GU2 7XH, United Kingdom.

https://doi.org/10.1016/j.physletb.2020.135626

Table 1
Summary of reaction properties. E_{beam} is the beam energy and $E_{c.m.}/V_B$ is the ratio of the reaction energy in the center-of-mass system (taking into account energy losses) to the calculated capture barrier V_B [42].

Reaction	CN	$Z_P Z_T$	V_B (MeV)	E_{beam} (MeV)	$E_{c.m.}/V_B$ (MeV)
^{64}Ni+^{238}U	^{302}120	2576	266.3	328-378	0.97-1.11
^{58}Fe+^{244}Pu	^{302}120	2444	253.8	307-351	0.97-1.11
^{54}Cr+^{248}Cm	^{302}120	2304	239.8	296-331	0.99-1.11
^{50}Ti+^{249}Cf	^{299}120	2156	225.3	264-289	0.96-1.05

In order to synthesize SHN, projectile and target nuclei must have sufficient energy to overcome the Coulomb barrier and form a composite system (capture), which must then evolve into a compact compound nucleus (CN) that survives fission. The resulting evaporation residue (ER) cross section of the compound nucleus at an excitation energy E^* can be described by the three-term expression

$$\sigma_{ER}(E^*) = \sum_L \sigma_{cap}(E^*, L) P_{CN}(E^*, L) W_{CN}(E^*, L), \quad (1)$$

where σ_{cap} is the capture cross section, P_{CN} is the probability for CN formation, and W_{CN} is the survival probability of the CN against fission through particle evaporation. E^* and L are the excitation energy and angular momentum of the CN, respectively.

The quasifission (QF) process, wherein the composite system fails to evolve into a CN after capture and reseparates into two fragments, occurs with probability $P_{QF} = 1 - P_{CN}$ [32,33]. In SHN-formation reactions, QF takes place within a few zeptoseconds (1 zeptosecond (zs) = 10^{-21} s) [32–35], faster than that of fission of the CN (fusion-fission, FF) and is the dominant process, thus severely hampering experimental efforts to produce SHN. P_{QF} depends sensitively on the reactant characteristics and can vary widely even for reactions that form the same CN (e.g., [36–38]). In-depth knowledge regarding the competition between FF and QF in SHN-formation reactions is therefore critical in order to validate and improve theoretical frameworks and thus provide reliable predictive power.

Angular distributions are a crucial characteristic of the QF process as they provide the most direct information regarding the contact time of the composite system. However, information regarding QF angular distributions for SHN-formation reactions is scarce: in the case of Z=120, only one data point has been previously measured for the ^{238}U+^{64}Ni reaction in inverse kinematics [32]. Mass and total-kinetic-energy (TKE) distributions of fission fragments have been measured for reactions using ^{64}Ni, ^{58}Fe and ^{50}Ti projectiles and actinide targets up to Cm (Z=96) at scattering angles of $\approx 90°$ [39–41] thus providing no direct information regarding rotation times. In this letter, we present QF mass and angular distributions for four Z=120-formation reactions measured with large angular coverage, where significant differences in reaction dynamics are observed through the QF outcomes.

2. Fission-fragment production and detection

2.1. Beam characteristics

Two experimental campaigns were performed at the Heavy Ion Accelerator Facility operated by the Australian National University in Canberra, Australia. Pulsed beams of ^{64}Ni, ^{58}Fe, ^{54}Cr and ^{50}Ti were delivered by the 14UD electrostatic accelerator coupled with the superconducting linear post-accelerator providing energies close to the interaction barriers [42]. A summary of reaction parameters is shown in Table 1.

2.2. Target fabrication

A 160-μg/cm^2 target of $^{238}UF_4$ on a 125-μg/cm^2 Al backing was used for the ^{64}Ni+^{238}U reactions. Targets of typically 0.1 mg/cm^2 (up to 0.6 mg/cm^2) of ^{244}Pu, ^{248}Cm and ^{249}Cf, isotopically enriched to levels $> 97\%$, were produced at the Johannes Gutenberg University Mainz via molecular plating [43]. Actinide material was deposited on the Ti side of backing foils fabricated at GSI Darmstadt that consisted of 230-250 μg/cm^2 Al with a 23-39 μg/cm^2 Ti layer on top. The targets were oriented such that the actinide material faced the incoming beam ions with their normal at 60° with respect to the beam direction to minimize the effects of the target thicknesses on the reconstruction of reaction kinematics. A carbon foil of thickness ∼40 μg/cm^2 was placed upstream of the targets to reduce contamination in the chamber from target material sputtered at backwards angles.

2.3. Experimental setup

Reaction products were detected using the CUBE spectrometer [44,45], comprising position-sensitive multi-wire proportional counters (MWPCs), configured such that the centers of two 28×36-cm^2 MWPCs were 195 and 180 mm from the target, at angles of (ϕ, θ)=(180°, 90°) (backwards) and (0°, 45°) (forwards), respectively. A recently-added third MWPC of size 13×36 cm^2 provided additional coverage at backwards angles, positioned with its normal at 135° at a distance of 180 mm from the target. Its angular coverage, subtended by the short dimension in the θ plane, was 139°-174° and 131°-169° for the first and second beamtime campaigns, respectively.

3. Data analysis methods

3.1. Event selection

An analysis using two-body kinematics was carried out for events measured in coincidence between the forward-angle MWPC and one of the two backward-angle MWPCs, allowing fission fragment mass ratios, defined as $M_R = m_1/(m_1 + m_2)$ (where m_1 and m_2 are the fragment masses at scission), and scattering angles to be determined. Event-by-event corrections for energy losses were applied iteratively, and three-body events (e.g., fissioning target-like nuclei following transfer reactions) were rejected by requiring that fragments were detected back-to-back in the center-of-mass frame. Further details of the experimental setup and analysis procedure are provided in references [44] and [45].

3.2. Mass-angle distributions (MADs)

Mass-angle distributions (MADs), defined as the center-of-mass scattering angle $\theta_{c.m.}$ versus the mass ratio M_R (see section 3.1), have been extensively used to probe QF and FF (e.g., [32,45–47]). Examples of MADs measured in this work can be found in Fig. 1(a)-(e). The color mappings represent the double-differential cross section $d^2\sigma/(d\theta_{c.m.} dM_R)$. Key features of experimental MADs include elastic and quasielastic scattering of target- and projectile-like fragments, which appear at mass ratios $M_R = m_T/(m_T + m_P)$ and $M_R = m_P/(m_T + m_P)$ (where m_T and m_P are the target and projectile masses, respectively), and fission fragments, which are expected to appear in the central region between the elastic components. The extent of the correlation between mass and angle reflects the system rotation, with significant correlations visible for rotations $\sim 180°$ or less. A lack of mass-angle correlation (i.e. a symmetric distribution centered at $M_R = 0.5$) indicates rotation angles of $> 360°$.

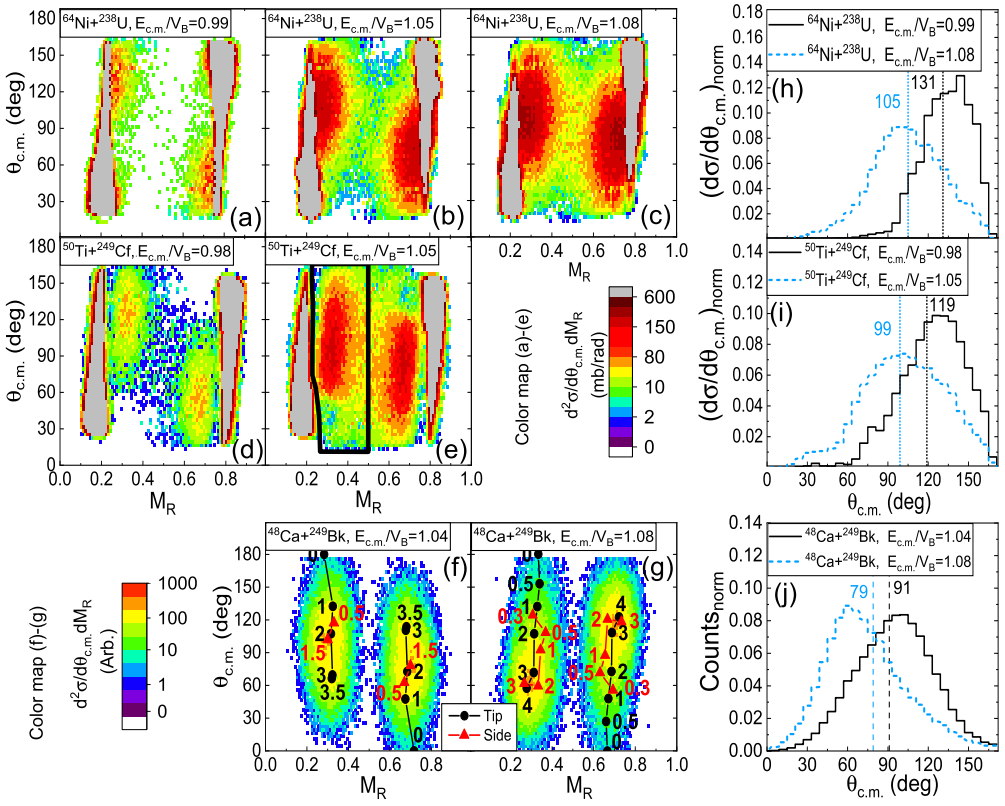

Fig. 1. (a)-(e) Experimental MADs. (f)-(g) MADs simulated from TDHF calculations [66]. Numbers overlaying the distributions indicate impact parameters in fm for tip (black circles) and side (red triangles) collisions. Color scales represent the double-differential cross section $d^2\sigma/(d\theta_{c.m.}dM_R)$. (h)-(i) Normalized experimental angular distributions of fission events (example region of fission events illustrated by black polygon in panel (e)). (j) Normalized angular distributions constructed from the TDHF predictions in panels (f)-(g). Labeled vertical dotted lines in (h)-(j) indicate the position of the weighted means as given by Eq. (2). In all panels, the reaction and ratio of the energy in the center-of-mass frame to the interaction barrier $E_{c.m.}/V_B$ is given, where V_B is calculated according to [42].

3.3. Angular distributions and mean scattering angles

In addition to MADs, changes in reaction dynamics can be studied in detail through 1-dimensional angular distributions of fission fragments, defined as the differential cross section $d\sigma/d\theta_{c.m.}$ as a function of center-of-mass angle $\theta_{c.m.}$. An example region of light fragments with $M_R < 0.5$ is marked by a black polygon in Fig. 1(e). Contributions from elastically-scattered target- and projectile-like fragments are minimized through a two-dimensional cut on $E_{K,exp}/E_{K,calc}$ versus M_R, where $E_{K,exp}$ are the measured total kinetic energies of the fragment pairs and $E_{K,calc}$ are the expected values for fission calculated following references [48] and [49]. Resultant angular distributions, found in Figs. 1(h) and (i), are normalized by the total integrated fission cross sections and quantified by their weighted means

$$\overline{\theta}_{c.m.} = \frac{\sum_{i=1}^{N} \theta_{c.m.,i}\,(d\sigma/dM_R)_i}{\sum_{i=1}^{N} (d\sigma/dM_R)_i}, \tag{2}$$

where N is the number of bins.

3.4. Extraction of contact times

Larger rotation angles of the intermediate system are associated with longer times before fragment separation and are, in general, indicative of more mass transfer and higher fusion probabilities. The angle of rotation $\Delta\theta$ in the center-of-mass frame between capture and reseparation is related to the contact time $t_{contact}$ through the simple relationship

$$\Delta\theta = t_{contact} \cdot \omega, \tag{3}$$

where $\omega = L/\mathcal{J}$ and L and $\mathcal{J}$ are the angular momentum and average moment of inertia (MoI), respectively. We convert mean scattering angles to contact times using the classical Monte Carlo model described in [35,45,50,51], which comprises the following components: angular momentum distributions for capture, the average MoIs during rotation, and classical Coulomb deflection angles on the incoming and outgoing trajectories. Angular momentum distributions were calculated using the coupled-channels code CCFULL [52], taking into account the appropriate static deformations and vibrational states [53–55].

Classical rigid-body moments of inertia, calculated assuming a spherical projectile touching the tip of a deformed target nucleus and normalized to the moment of inertia of a rigid sphere $\mathcal{J}_0 = \frac{2}{5}AR_0^2$ (where A is the mass of the composite system and $R_0 = 1.225A^{1/3}$ [56]), exhibit a parabolic dependence on the charge product of the reactants Z_PZ_T. More realistic estimates of $\mathcal{J}$ are obtained from the time-dependent Hartree-Fock (TDHF) framework and have been previously calculated for ^{34}S+^{232}Th [50] (Z_PZ_T=1440) and ^{64}Ni+^{238}U [57]. The resulting mean values of $\mathcal{J}/\mathcal{J}_0$ are $\sim$ 20% higher than the rigid-body calculations due to the dynamical evolution of the colliding nuclei after touching. We adopt the parabolic dependence of $\mathcal{J}/\mathcal{J}_0$ as a function of Z_PZ_T exhibited by the rigid-body approach to scale the TDHF predictions to the other relevant reactions.

4. Results and discussion

4.1. Experimental MADs

MADs measured for the ^{64}Ni+^{238}U and ^{50}Ti+^{249}Cf reactions are shown in Fig. 1(a)-(c) and (d)-(e), respectively. A very high

intensity of events originating mostly from scattered target and projectilelike fragments appear as expected at $M_R \approx 0.2$ and 0.8. The MADs obtained for ^{58}Fe+^{244}Pu and ^{54}Cr+^{248}Cm are qualitatively similar and are shown in the Supplemental Material [58]. The region $M_R \approx 0.25 - 0.75$, where fission fragments are expected, is dominated by mass-asymmetric events that peak at $M_R \approx 0.3$ and 0.7 in all experimental MADs. Such double-humped mass distributions with maxima close to doubly-magic ^{208}Pb fragments have been widely observed in studies involving heavy projectiles and actinide targets and are a typical signature of QF (e.g., [32,33,50,59–61]). No strong fission components with a symmetric mass split ($M_R = 0.5$) are visible.

4.2. Experimental angular distributions

A comparison of panels (a), (b) and (c) in Fig. 1 reveals fission events exhibiting an angular shift with changing energy. This behavior, evident for all of the reactions and possibly associated with changes in reaction dynamics, is investigated by examining angular distributions of light fragments with $M_R < 0.5$ as described in section 3.3. The resulting angular distributions for ^{64}Ni+^{238}U and ^{50}Ti+^{249}Cf found in Fig. 1(h) and (i), respectively, clearly demonstrate shifts in $\theta_{c.m.}$ as a function of energy. Values of the weighted means $\overline{\theta}_{c.m.}$, extracted using Eq. (2), are indicated by labeled vertical dotted lines in Fig. 1(h) and (i).

4.3. MADs simulated using time-dependent Hartree-Fock (TDHF) calculations

To aid the interpretation of the observed shifts in $\overline{\theta}_{c.m.}$, which could be associated with the contributing angular momenta and the contact time of the composite system, we examine recent work carried out within the fully-microscopic TDHF framework. This describes the dynamical evolution of the reactants, and has been used to investigate mass-angle correlations for heavy- and superheavy-element formation reactions (e.g., [62–65]). As a deterministic theory, TDHF calculations provide a single outcome for a given set of initial conditions. Values of M_R and $\theta_{c.m.}$ for specified impact parameters b (corresponding to different orbital angular momentum L) were calculated in reference [66] for the ^{48}Ca+^{249}Bk reaction. This system leads to the formation of ^{297}Ts and is more asymmetric than those measured here ($Z_P Z_T$=1940). Collisions occurring both at tip (axial) and side (equatorial) configurations were considered, since nuclear orientation effects are known to play an important role in QF dynamics involving deformed targets [44,67,68]. It has been suggested that P_{QF} is larger for collisions occurring at the tip of well-deformed targets and inhibited for collisions at the side [44,69,70], and that P_{CN} may even be enhanced in the more compact side orientations [68]. By taking the TDHF $(M_R, \theta_{c.m.})$ values calculated at center-of-mass energies of 211 and 218 MeV [66], we simulate MADs using an approach similar to that adopted in [63], wherein Gaussian distributions centered at each $(M_R, \theta_{c.m.})$ point were summed. Each Gaussian was weighted by $2L$+1 with a standard deviation in angle of 20° and a standard deviation in M_R that varies linearly from 0.025 at an initial mass split (corresponding to elastically-scattered projectile-like fragments) to 0.07 at $M_R = 0.5$ [45,63]. The simulated MADs, which underlay the TDHF outcomes in Fig. 1(f) and (g), are qualitatively similar to those obtained experimentally. More importantly, the TDHF predictions reproduce the trend of the angular shifts with energy apparent in the measured data, as can be seen explicitly in the $\theta_{c.m.}$ distributions (see Fig. 1(j)).

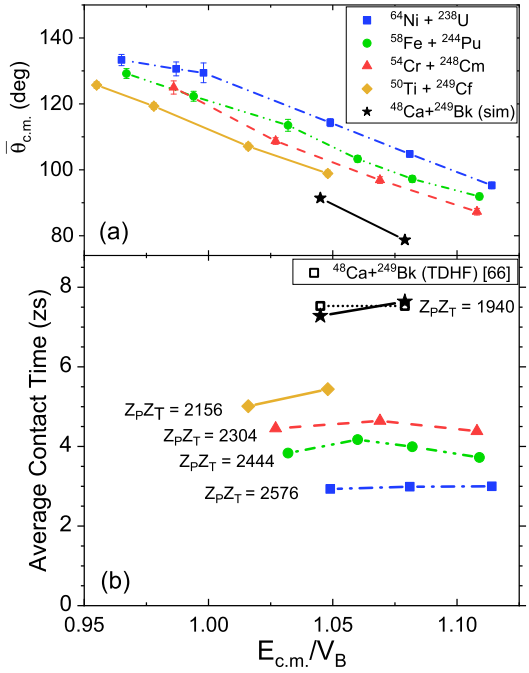

Fig. 2. (a) Dependence of mean scattering angles $\overline{\theta}_{c.m.}$ on $E_{c.m.}/V_B$. Black stars indicate $\overline{\theta}_{c.m.}$ values simulated from TDHF calculations for ^{48}Ca+^{249}Bk [66]. (b) Average contact times extracted using a classical Monte Carlo simulation. Black squares indicate direct TDHF predictions [66].

4.4. Evolution of mean scattering angles with energy and reactant characteristics

The experimental $\overline{\theta}_{c.m.}$ values shown in Fig. 2(a) exhibit a clear systematic picture of mean scattering angles that reduce with increasing $E_{c.m.}/V_B$. Moreover, we observe a well-pronounced systematic shift of mean angles dependent on the entrance channel; i.e., reactions with lower $Z_P Z_T$ (see Table 1) have lower values of $\overline{\theta}_{c.m.}$ than more symmetric reactions for any given value of $E_{c.m.}/V_B$. Mean scattering angles extracted from the MADs simulated using TDHF predictions for ^{48}Ca+^{249}Bk, also shown in Fig. 2(a), lie below those for ^{50}Ti+^{249}Cf as expected due to the increased asymmetry of the reactants, and follow the same trend with increasing energy. An equal weighting of tip and side collisions has been assumed; adjusting the tip:side ratio to 1:2 or 2:1 produces the same qualitative results.

4.5. Reaction contact times

In order to compare the reactions, differing entrance-channel properties (e.g., moments of inertia and angular momenta) must be taken into account. We therefore use the procedure detailed in section 3.4 to convert the mean scattering angles to contact times, defined as the time elapsed during the QF process between capture and the reseparation of fragments. In general, longer contact times should be associated with larger P_{CN} as the likelihood of reaching full dynamical equilibrium in all degrees of freedom increases with time. Indeed, events assumed to lead to fusion in the TDHF calculations for ^{48}Ca+^{249}Bk exhibit contact times of at least 25 zs, much longer than those resulting in QF [66].

Average contact times extracted from experimental $\overline{\theta}_{c.m.}$ values for data measured for energies above the interaction barriers (where orientation effects are averaged) are shown in Fig. 2(b). Although the angular distributions show that QF dominates the negligible FF components, the extracted timescales are associated with the sum of QF and FF as the mass region included in the angular distributions extends to symmetry (M_R=0.5). The times remain

relatively constant with increasing $E_{c.m.}/V_B$ despite the significant changes of mean scattering angles due to increasing angular momenta. Reactions with increasing entrance-channel asymmetry exhibit lengthening contact times, varying from ∼3 zs for ^{64}Ni+^{238}U to ∼5 zs for ^{50}Ti+^{249}Cf, and are in good agreement with the 3.1 zs estimated for the asymmetric mass component of the ^{238}U+^{64}Ni reaction by Tōke et al. [32]. Note that the relative trend is independent of the choice of model for $\mathcal{J}$, which affects absolute values. Contact times associated with the simulated ^{48}Ca+^{249}Bk angular distributions, which were also extracted using the classical Monte Carlo model, are represented by black stars in Fig. 2(b) and match well to the times predicted directly by the TDHF framework in reference [66] (black squares). Previous contact-time estimates for ^{64}Ni+^{238}U and ^{58}Fe+^{244}Pu made using mass and TKE measurements measured at ∼ 90° [40,60], employing the mass-drift formalism of reference [33], are ∼ 3 times shorter [71] than those extracted here.

5. Conclusions

To summarize, we have measured mass and angular distributions of fission fragments for four candidate reactions to be used for the synthesis of a new element with Z=120 at energies extending from below to ∼10% above the capture barriers. Well-pronounced mass-angle correlations, which evolve with the bombarding energies, were observed for all four reactions and are attributed to originate from changing reaction contact times, in agreement with predictions from TDHF calculations. Our results have revealed a systematic picture of contact times that increase with decreasing $Z_P Z_T$, with the longest exhibited for ^{50}Ti+^{249}Cf. The lengthening of contact times for increasingly asymmetric reactions suggest that the probability of fusion, wherein equilibration of all internal degrees of freedom must be reached, will also be increased. These results support the conclusion that, of the reactions studied here, ^{50}Ti+^{249}Cf has the highest fusion probability and is the most promising reaction for Z=120 formation.

Declaration of competing interest

The authors declare that they have no known competing financial interests or personal relationships that could have appeared to influence the work reported in this paper.

Acknowledgements

The authors would like to warmly thank Dr. T. Kibedi and all of the staff at the Heavy Ion Accelerator Facility operated by the Australian National University for their help with accelerator operations. We also acknowledge J. Steiner and V. Yakusheva for target preparations. This work was supported by the Australian Research Council via research grants DP140101377, DP160101254 and DP170102318, as well as through the German Academic Exchange Service (DAAD) via funds of the German Federal Ministry of Education and Research (BMBF). We also acknowledge the Australian Federal Government NCRIS program through the HIA capability for support of accelerator operations. Additionally, H.M. Albers, J. Khuyagbaatar, Ch.E. Düllmann and A. Yakushev would like to express their gratitude to the ANU for hosting them during beamtimes.

Appendix A. Supplementary material

Supplementary material related to this article can be found online at https://doi.org/10.1016/j.physletb.2020.135626.

References

[1] A. Sobiczewski, F.A. Gareev, B.N. Kalinkin, Phys. Lett. 22 (1966) 500.
[2] W.D. Myers, W.J. Swiatecki, Nucl. Phys. 81 (1966) 1.
[3] H. Meldner, Ark. Fys. 36 (1967) 593–598.
[4] G.A. Lalazissis, M.M. Sharma, P. Ring, Y.K. Gambhir, Nucl. Phys. A 608 (1996) 202.
[5] S. Ćwiok, J. Dobaczewski, P.H. Heenen, P. Magierski, W. Nazarewicz, Nucl. Phys. A 611 (1996) 211.
[6] K. Rutz, M. Bender, T. Bürvenich, T. Schilling, P.G. Reinhard, J.A. Maruhn, W. Greiner, Phys. Rev. C 56 (1997) 1.
[7] M. Bender, K. Rutz, P.G. Reinhard, J.A. Maruhn, W. Greiner, Phys. Rev. C 60 (1999) 034304.
[8] A.T. Kruppa, M. Bender, W. Nazarewicz, P.G. Reinhard, T. Vertse, S. Ćwiok, Phys. Rev. C 61 (2000) 034313.
[9] Y.T. Oganessian, et al., Eur. Phys. J. A 5 (1999) 63.
[10] Y.T. Oganessian, et al., Phys. Rev. C 70 (2004) 064609.
[11] Y.T. Oganessian, et al., Phys. Rev. C 74 (2006) 044602.
[12] Y.T. Oganessian, J. Phys. G, Nucl. Part. Phys. 34 (2007) R165.
[13] S. Hofmann, et al., Eur. Phys. J. A 32 (2007) 251.
[14] L. Stavsetra, K.E. Gregorich, J. Dvorak, P.A. Ellison, I. Dragojević, M.A. Garcia, H. Nitsche, Phys. Rev. Lett. 103 (2009) 132502.
[15] Y.T. Oganessian, et al., Phys. Rev. Lett. 104 (2010) 142502.
[16] R. Eichler, et al., Radiochim. Acta 98 (2010) 133.
[17] Ch.E. Düllmann, et al., Phys. Rev. Lett. 104 (2010) 252701.
[18] P.A. Ellison, et al., Phys. Rev. Lett. 105 (2010) 182701.
[19] J.M. Gates, et al., Phys. Rev. C 83 (2011) 054618.
[20] S. Hofmann, et al., Eur. Phys. J. A 48 (2012) 62.
[21] A. Yakushev, et al., Inorg. Chem. 53 (2014) 1624.
[22] D. Rudolph, et al., Phys. Rev. Lett. 111 (2013) 112502.
[23] J. Khuyagbaatar, et al., Phys. Rev. Lett. 112 (2014) 172501.
[24] D. Kaji, et al., J. Phys. Soc. Jpn. 86 (2017) 034201.
[25] J. Roberto, et al., Nucl. Phys. A 944 (2015) 99.
[26] S. Hofmann, et al., GSI Scientific Report-2007, 131, 2008.
[27] Y.T. Oganessian, et al., Phys. Rev. C 79 (2009) 024603.
[28] S. Hofmann, et al., GSI Scientific Report-2011, 205, 2012.
[29] S. Hofmann, et al., Eur. Phys. J. A 52 (2016) 180.
[30] J. Khuyagbaatar, et al., GSI Scientific Report-2012, 131, 2013.
[31] Ch.E. Düllmann, et al., in preparation.
[32] J. Tōke, R. Bock, G.X. Dai, A. Gobbi, S. Gralla, K.D. Hildenbrand, J. Kuzminski, W.F.J. Müller, A. Olmi, H. Stelzer, Nucl. Phys. A 440 (1985) 327.
[33] W.Q. Shen, et al., Phys. Rev. C 36 (1987) 1.
[34] D.J. Hinde, D. Hilscher, H. Rossner, B. Gebauer, M. Lehmann, M. Wilpert, Phys. Rev. C 45 (1992) 1229.
[35] R. du Rietz, D.J. Hinde, M. Dasgupta, R.G. Thomas, L.R. Gasques, M. Evers, N. Lobanov, A. Wakhle, Phys. Rev. Lett. 106 (2011) 052701.
[36] D.J. Hinde, et al., Phys. Rev. Lett. 89 (2002) 282701.
[37] M.G. Itkis, I.M. Itkis, G.N. Knyazheva, E.M. Kozulin, Nucl. Phys. A 834 (2010) 374.
[38] J. Khuyagbaatar, et al., Phys. Rev. C 97 (2018) 064618.
[39] M.G. Itkis, et al., Nucl. Phys. A 734 (2004) 136–147.
[40] M.G. Itkis, et al., Nucl. Phys. A 787 (2007) 150c–159c.
[41] E.M. Kozulin, et al., Phys. Lett. B 686 (2010) 227–232.
[42] W.D. Myers, W.J. Świątecki, Phys. Rev. C 62 (2000) 044610.
[43] J. Runke, et al., J. Radioanal. Nucl. Chem. 299 (2014) 1081.
[44] D.J. Hinde, et al., Phys. Rev. C 53 (1996) 1290.
[45] R. du Rietz, et al., Phys. Rev. C 88 (2013) 054618.
[46] R. Bock, et al., Nucl. Phys. A 388 (1982) 334.
[47] J. Khuyagbaatar, et al., Phys. Rev. C 91 (2015) 054608.
[48] V.E. Viola, K. Kwiatkowski, M. Walker, Phys. Rev. C 31 (1985) 1550.
[49] D.J. Hinde, J.R. Leigh, J.J.M. Bokhorst, J.O. Newton, R.L. Walsh, J.W. Boldeman, Nucl. Phys. A 472 (1987) 318.
[50] E. Prasad, et al., Phys. Rev. C 93 (2016) 024607.
[51] E. Prasad, et al., Phys. Rev. C 96 (2017) 034608.
[52] K. Hagino, et al., Comput. Phys. Commun. 123 (1999) 143.
[53] T. Kibédi, R.H. Spear, At. Data Nucl. Data Tables 80 (2002) 35.
[54] P. Möller, A.J. Sierk, T. Ichikawa, H. Sagawa, At. Data Nucl. Data Tables 109 (2016) 1.
[55] B. Pritychenko, M. Birch, B. Singh, M. Horoi, At. Data Nucl. Data Tables 107 (2016) 1.
[56] M.B. Tsang, H. Utsunomiya, C.K. Gelbke, W.G. Lynch, B.B. Back, S. Saini, P.A. Baisden, M.A. McMahan, Phys. Lett. B 129 (1983) 18.
[57] K. Sekizawa, K. Yabana, Phys. Rev. C 93 (2016) 054616.
[58] See Supplemental Material at https://doi.org/10.1016/j.physletb.2020.135626, for all experimental mass-angle distributions.
[59] K. Nishio, et al., Phys. Rev. C 86 (2012) 034608.

[60] E.M. Kozulin, et al., Phys. Rev. C 94 (2016) 054613.
[61] D.J. Hinde, et al., Phys. Rev. C 97 (2018) 024616.
[62] C. Simenel, D.J. Hinde, R. du Rietz, M. Dasgupta, M. Evers, C.J. Lin, D.H. Luong, A. Wakhle, Phys. Lett. B 710 (2012) 607.
[63] A. Wakhle, et al., Phys. Rev. Lett. 113 (2014) 182502.
[64] K. Hammerton, et al., Phys. Rev. C 91 (2015) 041602.
[65] C. Simenel, A.S. Umar, Prog. Part. Nucl. Phys. 103 (2018) 19.
[66] A.S. Umar, V.E. Oberacker, C. Simenel, Phys. Rev. C 94 (2016) 024605.
[67] D.J. Hinde, et al., Phys. Rev. Lett. 100 (2008) 202701.
[68] D.J. Hinde, M. Dasgupta, J.R. Leigh, J.P. Lestone, J.C. Mein, C.R. Morton, J.O. Newton, H. Timmers, Phys. Rev. Lett. 74 (1995) 1295.
[69] S. Mitsuoka, H. Ikezoe, K. Nishio, J. Lu, Phys. Rev. C 62 (2000) 054603.
[70] S. Mitsuoka, H. Ikezoe, K. Nishio, K. Satou, J. Lu, Phys. Rev. C 65 (2002) 054608.
[71] G.N. Knyazheva, I.M. Itkis, E.M. Kozulin, J. Phys. Conf. Ser. 515 (2014) 012009.